Journal of Theoretical Biology 380 (2015) 83–97

Contents lists available at ScienceDirect

Journal of Theoretical Biology

journal homepage: www.elsevier.com/locate/yjtbi

Global contraction or local growth, bleb shape depends on more than just cell structure

Thomas E. Woolley*, Eamonn A. Gaffney, James M. Oliver, Sarah L. Waters, Ruth E. Baker, Alain Goriely

University of Oxford, Andrew Wiles Building, Radcliffe Observatory Quarter, Woodstock Road, Oxford, OX2 6GG, United Kingdom

HIGHLIGHTS

- Pressure driven protrusions aid motility in muscle stem cells.
- Cell shape is replicated using a mechanical model of membrane, cortex and adhesions.
- Observed protrusions, with small neck regions, are difficult to reproduce.
- Localised membrane growth and cortex contraction stabilise the neck region.

ARTICLE INFO

Article history:
Received 27 August 2014
Received in revised form
20 January 2015
Accepted 18 April 2015
Available online 29 April 2015

PACS:
46.05.+b
46.90.+s
87.10.Pq
87.17.Aa
92B05
92C10
74L15

Keywords:
Blebbing
Solid mechanics
Membrane dynamics
Cortex structure
Ezrin adhesions

ABSTRACT

When the plasma membrane of a cell locally delaminates from its actin cortex the membrane is pushed outwards due to the cell's internal fluid pressure. The resulting spherical protrusion is known as a bleb. A cell's ability to function correctly is highly dependent on the production of such protrusions with the correct size and shape. Here, we investigate the nucleation of large blebs from small, local neck regions. A mathematical model of a cell's membrane, cortex and interconnecting adhesions demonstrates that these three components are unable to capture experimentally observed bleb shapes without the addition of further assumptions. We have identified that combinations of global cortex contraction and localised membrane growth are the most promising methods for generating prototypical blebs. Currently, neither proposed mechanism has been fully tested experimentally and, thus, we propose experiments that will distinguish between the two methods of bleb production.

1. Introduction

Cell shape and function are highly correlated (Singhvi et al., 1994). The ability of an animal cell to produce large and dynamic conformational changes allows the cell to undergo many different phenomena, such as growth (Folkman and Moscona, 1978) and motion (Köppen, 2006). Equally, structural abnormalities in cells are seen in many pathologies, including cancer and cardiomyopathies (Phillips et al., 2007). Although cell shape may change passively in response to external forces, we are interested in active cellular deformation, through which we gain a better understanding of how the previously mentioned phenomena are controlled.

We focus our attention on understanding how cellular shape is controlled in a specific form of deformation known as blebbing, whereby a cell's membrane delaminates from its actin skeleton leading to the creation of multiple, spherical protrusions (see Figs. 1 and 2(a)) (Charras, 2008). Blebs play an important role in a number of cellular phenomena including mitosis and locomotion in tumour and embryonic cells (Otto et al., 2011; Sahai and Marshall, 2003; Cunningham, 1995). In particular, our investigation considers muscle satellite stem cells that are able to use blebs to migrate along muscle fibres in order to find, and repair, sites of

* Corresponding author.
E-mail address: woolley@maths.ox.ac.uk (T.E. Woolley).

http://dx.doi.org/10.1016/j.jtbi.2015.04.023
0022-5193/

tissue damage. Critically, bleb size is very important in the case of healing muscle as it has been shown that if a satellite cell's blebs are too big or too small, the cell is no longer able to use them to move (Collins-Hooper et al., 2012).

In this paper we aim to elucidate the mechanisms that are crucial for the maintenance of blebs that grow to have radii larger than the neck widths that connect the bleb to the cell, as seen in Fig 1. In order to consider bleb morphologies we extend a previously developed solid mechanics blebbing model (Woolley et al., 2014a, 2014b) to include effects from the cell membrane, the cytoskeletal cortex and interconnecting adhesions. This model allows us to pay close attention to the peeling of membrane away from the cortex and stabilisation of the bleb's neck, which has not previously been modelled in great detail. We want to understand this peeling phenomenon as it will provide insights into the control of bleb shape, which is very important for correct cellular behaviour and their ability to heal damaged muscle.

Throughout this paper we will often refer to the blebs highlighted in Fig. 1 as small-necked blebs. Specifically, these are blebs with a rounded morphology such that their neck width is smaller than the bleb's maximal width (see Fig. 2(a)). These small-necked blebs are further separated into categories of small-necked-big blebs and small-necked-small blebs. A small-necked-big bleb is any small-necked bleb that extends more than 1.5 μm (which are commonly seen on muscle stem cells), whereas small-necked-small blebs have an extension smaller than 1.5 μm (more commonly seen in amniotic stem cells). This terminology will aid later on when we see that different mechanisms are able to explain different sizes of small-necked blebs.

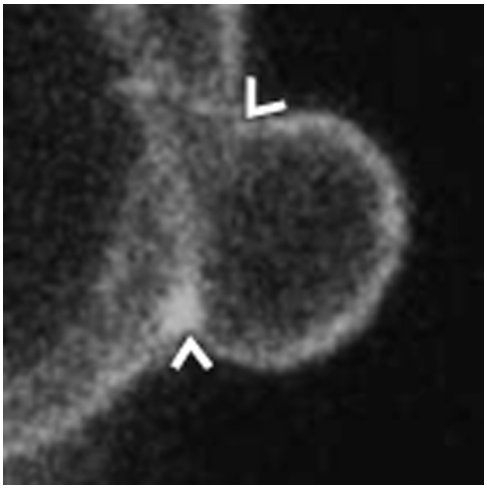

Fig. 1. Single confocal microscopy slice of a muscle satellite stem cell; used with permission from the Skeletal Muscle Development Group, University of Reading. The fluorescence highlights polymerised actin. Notice the commonly seen acute angle, highlighted by the white arrow heads, between the cell body and the bleb.

Critically, not only are small-necked blebs important in terms of cellular motion but they also present an interesting phenotype as the acute angle between the cell body and the bleb suggests that they are difficult to maintain. Generally, we would expect the membrane to continue tearing away from the cortex, leaving only a large-necked protrusion, as shown in Fig. 2(b). Indeed, as we will see later in the Results section and Appendices, simple generic mechanisms are unable to reproduce the small-neck-bleb morphology.

1.1. Biological background

Although blebbing is an extremely complex behaviour the structural shape of a cell is thought to depend on three components: a flexible lipid bilayer membrane, a stiff actin cortex and adhesion proteins that couple these two structures (Charras et al., 2008). Initially, blebs have no internal actin cortex structure, their formation is driven by intracellular pressure being larger than the extracellular pressure. After 10-30 s the expansion phase of the bleb stops and cortex is able to reform within the bleb. Over a much longer timescale of 1–2 min the newly formed cortex contracts and deforms causing the bleb to be retracted. This allows the blebbing cycle to begin again. Occasionally, instead of retracting the bleb, a cell may produce further blebs on this new protrusion, which has been stabilised by the re-formation of actin. When blebs form on existing blebs long lobopodia-like structures can be created (Charras and Paluch, 2008).

The adhesion proteins that link the cortical cytoskeleton to the plasma membrane are thought to be members of the highly conserved ezrin–radixin–moesin (ERM) family (Tsukita et al., 1997). Ezrin is the most studied protein of this family and, due to the structural similarities between the proteins, it is thought to be a good indicator for the properties and functions of the other members (Bretscher et al., 1997). Based on the experimental work of Liu et al. (2007), we postulate that the adhesion molecules behave mechanistically as piecewise springs, in that their resistive force is proportional to their length, until a critical extension. Beyond this critical length the adhesion molecules detach from the membrane, disconnecting the cortex from the membrane.

1.2. Mathematical background

Mathematical models of blebbing that encapsulate a large range of specific phenomena have been previously developed (Tinevez et al., 2009; Strychalski and Guy., 2012). The models span the entire range of complexity, from very simple geometric descriptions of blebbing modelled as two spherical caps (Hu, 2009) to multiscale, agent-based approaches (Tozluoğlu et al., 2013); see Woolley et al. (2014b) for a general review. Here, we

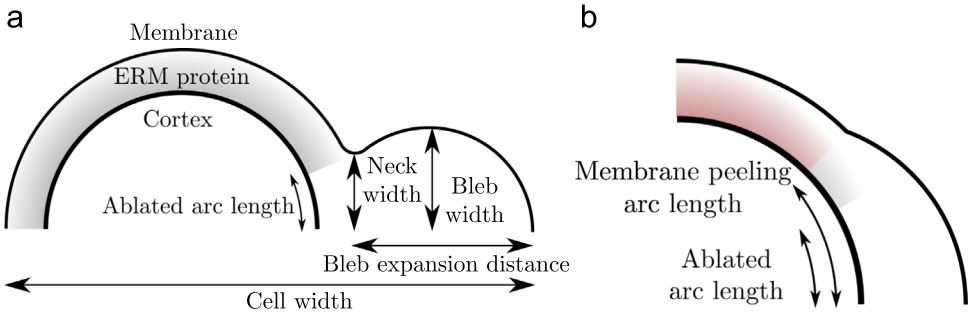

Fig. 2. Schematic diagram of a blebbing cell illustrating the profile of (a) small-necked bleb and (b) large-necked protrusion and other defined nomenclature. The shaded region shows where ERM adhesions are present.

focus on the peeling of the membrane away from the cortex and stabilisation of the bleb's neck in order to maintain small-necked blebs. We are interested in understanding the peeling phenomenon and its relationship with bleb size because of its implications on cellular motion.

Previously Woolley et al. (2014a,b) modelled a cell's membrane and cortex as a composite material using an extensible, axisymmetric, elastic shell. In order to investigate the membrane–cortex peeling phenomenon the previous composite body model is now extended to include the membrane and cortex as separate entities, with the addition of adhesion forces that attach the two structures together.

Using Fig. 2 we define various terms, which aid the discussion of a blebbing cell's geometry. The ablated arc length is the region over which adhesions are first removed either numerically, or experimentally. This ablation region mimics the experiments of Tinevez et al. (2009), where a laser was used to initiate bleb formation by locally destroying the cortex, thereby removing the adhesions. Outside of this ablated region the membrane is initially fully adhered to the cortex. However, as illustrated in Fig. 2(b), further breaking of adhesions can occur, causing more membrane to be released from the cortex.

Having set the nomenclature we begin in Section 2 by introducing the reconfiguring shell model and extending it to include cortex–membrane adhesions. The initial results in Section 3, as well as the negative results in Appendices C–H, demonstrate that small-necked blebs are not easy to produce in the model. Critically, it is not obvious *a priori* that so many of the suggested mechanisms should provide negative results. Thus, the Appendices are maintained in order to transparently display the large number of numerical experiments that were done. We conclude Section 3 by demonstrating that global cortex contraction and local membrane growth are able to reproduce the small-necked-bleb phenomenon, even though they are extremely different mechanisms. Finally, after summarising the results in Section 4, we provide experimentalists with a set of testable hypotheses that would allow us to identify which of the two successful mechanisms is dominant.

2. Mathematical system

The geometry and shell mechanics (Evans and Skalak, 1980) are defined as in previous articles (Woolley et al., 2014a,b). The pertinent equation system is briefly recapitulated here and explained below. Further details and boundary conditions can be found in Appendix A.

The equations are the following:

$$\frac{\partial y}{\partial \sigma} = \lambda_s \cos(\theta), \tag{1}$$

$$\frac{\partial \theta}{\partial \sigma} = \lambda_s \kappa_s, \tag{2}$$

$$\frac{\partial z}{\partial \sigma} = -\lambda_s \sin(\theta), \tag{3}$$

$$\frac{\partial s}{\partial \sigma} = \lambda_s, \tag{4}$$

$$\frac{\partial T_s}{\partial \sigma} = \lambda_s (t_\phi \cos(\theta) + FCy \sin(\delta - \theta) + Q\kappa_s), \tag{5}$$

$$\frac{\partial Q_s}{\partial \sigma} = \lambda_s (\Delta P y - \kappa_\phi y t_\phi - \kappa_s T_s - FCy \cos(\delta - \theta)), \tag{6}$$

$$\frac{\partial \kappa_s}{\partial \sigma} = \frac{\lambda_s}{y}\left(\cos(\theta)(\kappa_s - \kappa_\phi) - \frac{Q_s}{M}\right), \tag{7}$$

$$F(\sigma) = \kappa E(\sigma), \tag{8}$$

$$E(\sigma) = \left(\sqrt{(z(\sigma) - r_c \cos(\sigma/\rho))^2 + (y(\sigma) - r_c \sin(\sigma/\rho))^2} - (\rho - r_c)\right), \tag{9}$$

$$\tan(\delta) = \frac{y(\sigma) - r_c \sin(\sigma/\rho)}{z(\sigma) - r_c \cos(\sigma/\rho)}, \tag{10}$$

where

$$\kappa_\phi = \frac{\sin(\theta)}{y}, \tag{11}$$

$$t_s = A\left(\lambda_s^2 + \mu\left(\frac{y}{y_{rc}}\right)^2 - (1+\mu)\right), \tag{12}$$

$$t_\phi = A\left(\mu\lambda_s^2 + \left(\frac{y}{y_{rc}}\right)^2 - (1+\mu)\right). \tag{13}$$

Eqs. (1)–(4) define the axisymmetric geometry of the cell shape with the z-axis being the axis of rotational symmetry and the azimuthal angle being denoted ϕ (see Fig. 3). A membrane reference configuration, (z_{rc}, y_{rc}), is constructed which corresponds to an unstressed state. This is the state in which the pressure difference, ΔP, across the membrane and the surface tension are both zero. This reference configuration is parameterised by its arc length, σ, which is measured

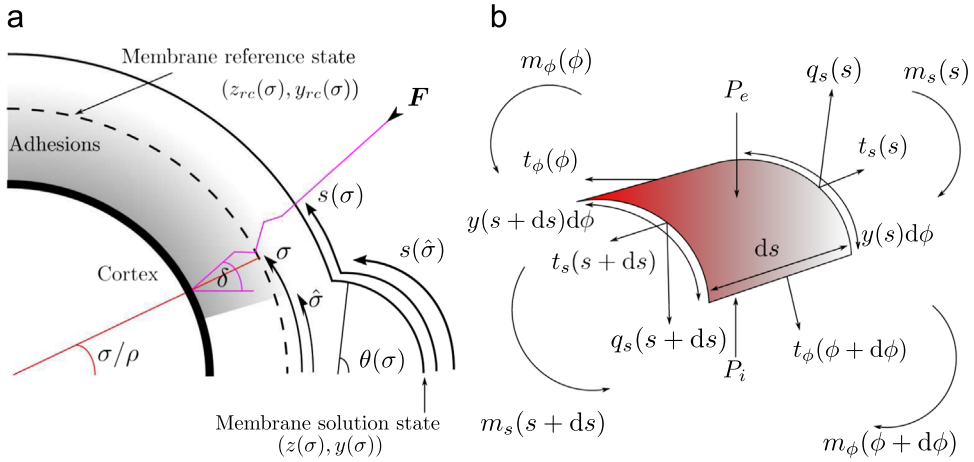

Fig. 3. Diagram of stresses and moments acting on the cell membrane. (a) Definition of geometric variables and adhesion forces. (b) A small section of the membrane on which the stresses are defined.

from the intercept of the reference configuration with the z-axis. We choose an initial reference configuration to be a sphere of radius ρ, thus $\sigma \in [0, \rho\pi]$.

The y and z variables are the solution configuration coordinates, representing the shape of reference configuration once it has been pressurised. The variable s measures the arc length of the solution configuration. The final geometric variable, θ, is the outward pointing normal angle of the membrane solution configuration, measured anticlockwise from the z-axis. Using Fig. 3, we are able to rigorously define the features presented in Fig. 2. The point, along the arc length, at which the membrane transitions from adhered to the cortex to unadhered is $\hat{\sigma}$. The neck width is $y(\hat{\sigma})$. The bleb expansion distance is $z(0)-z(\hat{\sigma})$ and, finally, the widest point of the bleb satisfies $\partial y/\partial z = 0$, if it is a small-necked bleb, otherwise the widest point is at $y(\hat{\sigma})$.

The reference and solution membrane configurations are related via the following stretch ratio:

$$\lambda_\phi = \frac{y(\sigma)}{y_{rc}(\sigma)}, \tag{14}$$

which is the *radial stretch ratio* that measures the axisymmetric deformation. Similarly, λ_s, defined by Eq. (4), is the *arc length stretch ratio*, which characterises the local stretching of the body coordinates with respect to arc length. Finally, in order to complete the geometric definition (7) and (11) define the principal curvatures of an axisymmetric surface, κ_s and κ_ϕ, respectively.

Eqs. (5)–(6) define the force balances on the pressurised membrane. In order to balance the pressure difference, the shell supports surface tensions, t_s and t_ϕ. Further, because we assume that the shell can support bending, we define M to be the membrane bending modulus and note that there may be non-zero normal shear stresses, q_s, which act along the membrane's normal direction (see Fig. 3(b)). Notice that we formulate the model in terms of $T_s = y t_s$ and $Q_s = y q_s$. This simple transformation allows us to remove singularities from all but one equation, which facilitates efficient numerical simulation of the system.

Eqs. (8)–(10) define the influence of the adhesion force, $\boldsymbol{F}$, on the system (Fig. 3(a)). Initially, we model the adhesions as Hookean springs. The springs have a spring constant, κ, which measures the extension of a given adhesion for a given load (Liu et al., 2007). Since κ is measured per adhesion it is multiplied by an adhesion concentration, C, providing a force per area, which counter-acts the pressure gradient. The adhesion concentration can be gained from data on the density of ERM proteins connecting the cortex to the membrane (Tozluoğlu et al., 2013). The parameter grouping κC will be of interest later and is called the adhesion strength density and has units pN/μm^3. Although we initially treat κC as a constant we relax this condition later, when peeling is considered.

Note that adhesion forces are directed along the material point trajectory. Specifically, this means the adhesions remain adhered to the same material point on the membrane throughout the deformation. Since the initial reference membrane and cortex are concentric spheres of radii ρ and r_c, respectively, the adhesions are connected normally to both surfaces. By fixing the end locations of the adhesion springs we are able to use Eq. (10) to calculate the angle, δ, along which the force is directed (Fig. 3(a)).

Finally, Eqs. (12) and (13) are constitutive laws linking stresses and strains in the membrane. The parameter A characterises the elastic properties of the membrane and μ measures the relative extensibility of the membrane in the azimuthal and longitudinal directions (Evans and Skalak, 1980).

In order to mimic the adhesion ablation experiments we reduce the adhesion strength density over an ablated arc length (see Fig. 2), whilst the reference configuration is kept fixed. This captures the near instantaneous action of the laser used in the experiment, which destroys the cortex locally. After this initial ablation of adhesions the membrane deformation arises through reference configuration remodelling. This means that the arc length and profile of the reference configuration are able to update according to some postulated evolution rule modelling growth of the membrane. Extended discussion on the update rule can be found in Appendix A.2.

As the simulation progresses it may occur that the membrane and cortex move away from each other, causing the adhesions that couple them to stretch beyond the critical length, E_c. Adhesions that stretch beyond the critical length are considered to be broken, which is enforced through the adhesion density, $C(\sigma)$, as discussed in Appendix A.3. Effectively, C is a scaled Heaviside function, which is zero in the unadhered region and a non-zero constant in the adhered region. The transition point, $\hat{\sigma}$, increases as the membrane peels away from the cortex, thus, increasing the region over which C is zero and, therefore, increasing the region which is unadhered.

3. Results

We begin by presenting the base case simulation, which combines only effects of membrane growth and adhesion tearing. The protrusions produced in this scenario illustrate our main concern that the blebs do not maintain a small neck, rather the membrane tears away from the cortex producing a large-necked bleb. We seek to produce the desired small-necked bleb form by perturbing the base case in various ways. These perturbations allow us to investigate which factors dominate the neck width of the final profile. Although all of these perturbations have the potential to produce small-necked blebs when used in conjunction with thought experiments, or verbal models, we demonstrate that the only mechanisms that can account for the small-necked-bleb morphology involve global cortex contraction, or local membrane growth. All of the negative results have been relegated to Appendices C–H.

In all solutions, unless otherwise stated, the parameters are $A = 400$ pN/μm, $M = 10^{-2}$ pN μm, $E_c = 40$ nm, $\kappa C = 10^3$ pN/μm^3 and ΔP is initially 20 pN/μm^2. The parameter values have been taken from a wide range of blebbing and membrane literature (Liu et al., 2007; Nichol and Hutter, 1996; Dai and Sheetz, 1999; Sheetz et al., 2006; Pozrikidis, 2001; Collins-Hooper et al., 2012) and offer an order of magnitude estimate, if not an exact value.

3.1. Base case

In this simulation adhesions break if they exceed their critical length and membrane grows wherever the adhesions are broken, as defined in the algorithm presented in Appendix A.3. Fig. 4 clearly shows that as the simulation progresses adhesions break, causing the membrane and cortex to separate. Accordingly, the membrane peels away from the cortex and produces a neck width that is far too large for the muscle stem cell blebs that we are considering, although cells producing blebs with such wide necks do exist (Maugis et al., 2010).

The solution profile shape is primarily driven by the balance between the resistive force per area produced by the adhesions and the pressure difference. As the membrane peels back along the cortex more of the membrane is able to grow, causing the reference configuration to become larger (see Eqs. (A.10) and (A.12)). Because the solution volume is constant the growing reference configuration causes the pressure to drop. As the pressure drops the adhesions pull the membrane closer to the cortex. Eventually, the pressure in the cell drops sufficiently, such that the remaining adhesions are all below the critical breaking length. These processes, which lead to a reduction in pressure difference, are similar to those that occur in the case where the adhesions do not break (illustrated in Appendix B):

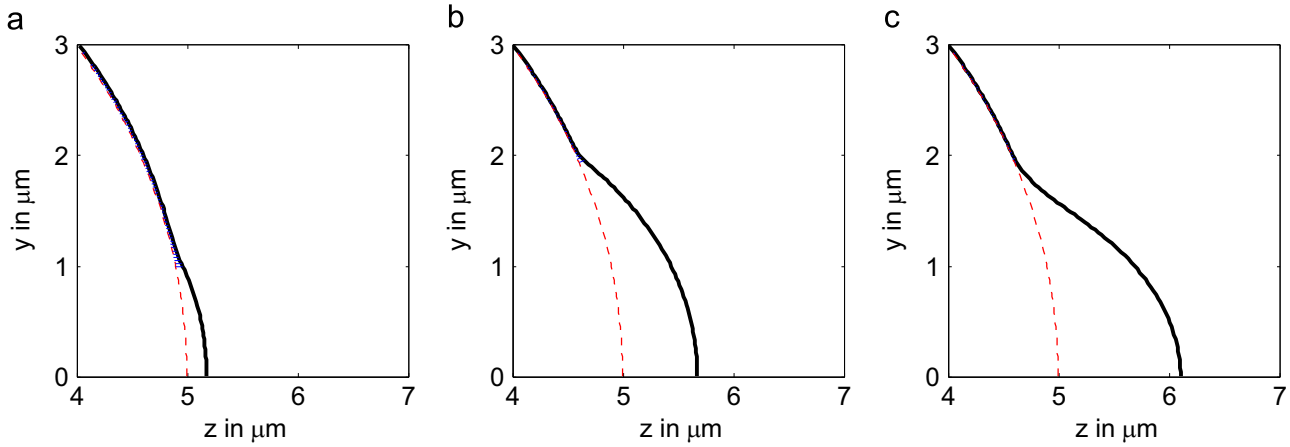

Fig. 4. Evolution of the base case simulation. In this, and all future profiles, the cell plotting scheme remains the same. The dashed (red) hemisphere denotes the cortex. The thick (black) curve above this represents the membrane. The thin (blue) lines between the cortex and membrane curves represent the adhesions. (a) The initialisation curve is the same as in Fig. A1(b) in Appendix A.3. (b) The solution profile state at which adhesions stop breaking. (c) The solution profile after a large number of iterations. The simulation was allowed to continue until the difference between consecutive solution pressure differences was less than 10^{-5} pN/μm^2. The equilibrium pressure differences are (b) $\Delta P = 4.3$ pN/μm^2 and (c) $\Delta P = 0.03$ pN/μm^2. All other parameters and stages in the iteration are as in Fig. A1. (For interpretation of the references to colour in this figure caption, the reader is referred to the web version of this paper.)

although adhesions at the start of the simulation are above the critical length, by the end of the simulation all adhesions are below the critical length, because of the reduction in pressure. This can be seen in Fig. 4(b), where the pressure difference has dropped from 20 pN/μm^2 to 4 pN/μm^2. Not only does this mean that no more tearing occurs, but it also suggests that, unless the cell is repressurised through some method, the cell would struggle to create another protrusion.

Clearly, we have illustrated our primary point that maintaining a small neck width cannot be explained with this simple model. Indeed, the action of adhesion breaking and membrane growth do not generally allow the production of small-necked blebs. Compare this to the simulations in Appendix B, which, although unphysical (as adhesion breaking is suppressed), demonstrate the profile shape we are interested in producing.

3.2. Perturbing the base case

For simplicity, we try to produce small-necked blebs by perturbing different structural aspects contained within this basic membrane–cortex–adhesion framework. For example: altering the membrane stiffness ratio; changing the membrane growth time scale; increasing the adhesion strength density; making the adhesion density profile stochastic; generalising the adhesions force–extension curve to be non-linear; or varying the angle along which the adhesions stretch are all theoretical ways that could result in the creation of small-necked-large blebs. Unfortunately, these perturbations are unable to reproduce the experimentally seen results, as discussed in Appendices C, D, E, F, G and H, respectively.

Having seen that alterations to the static structural properties of the membrane and adhesions are unable to reproduce experimentally observed small-necked-big blebs we include additional evolving mechanisms that are able to produce the desired small-neck features.

3.2.1. Localised growth

In all other simulations membrane growth occurs wherever the membrane has broken free of the cortex, see Appendix A.2. In this section we fix the region over which growth is allowed to occur. The simulation iteration steps are very similar to the base case. The only difference being that the region of growth is fixed at a particular arc length. Although it may be questioned whether such a mechanism can act locally preliminary experimental work suggests that membrane vesicles are locally recruited to the blebs (Patel and Dash, 2013). However, the direction of cause and effect between blebbing and local membrane recruitment is unclear.

Simulations, illustrated in Fig. 5, demonstrate the evolution of the profile and adhesion extensions as growth occurs only within the initial adhesion ablated region $\sigma \in [0, 1]$ μm. The bottom row illustrates that the adhesions are able to break as normal. Initially, unadhered membrane corresponds exactly to the region over which membrane is also growing. However, as seen in the bottom plot of Fig. 5(a), a number of the adhesions are beyond the critical length. By the time the simulation has reached Fig. 5(b) all remaining adhesions are below the threshold length, but the local growth has created three regions of different behaviours. For $\sigma \in [0, 1]$ μm the membrane is reconfiguring and unadhered, this leads to the production of a large protrusion; for $\sigma \in (1, \hat{\sigma}]$ μm the membrane is unadhered but does not grow and, so, it can only sustain a small deflection from the cortex; the rest of the cell's membrane is adhered to the cortex and is pulled closer to the cortex, by the adhesions, as pressure decreases. Fig. 5(c) illustrates that not only are small-necked blebs possible, but also the outer region deflection has decreased, causing the cortex and membrane to be within the critical adhesion length. As these two regions are now closer adhesions would be able to reform in the outer region, causing the membrane and cortex to be attached once more. Finally, the local growth mechanism has a further beneficial aspect. Due to the adhesions breaking in a region around the protrusion, bleb activity would be promoted within this small localised region. This promotion could act as a form of polarisation.

3.2.2. Cortex contraction

Until now the cortex has been modelled as a rigid permeable structure, whose only function has been a location on which one side of the adhesion proteins are fixed. However, the intracellular pressure may act on the cortex as well as the membrane. Hence, as the pressure is released by the bleb, we may expect some contraction in the cortex. Despite this, contraction of the entire cortex is a global phenomenon, which has not been reported in the muscle stem cell blebbing literature and may be at odds with the current knowledge of blebs being localised protrusions. The mathematical formulation of the contraction can be found in

Appendix K. The resulting simulations, illustrated in Fig. 6, demonstrate that small-necked-large blebs are produced (Fig. 6(a) and (b), compare with the simulations in Appendix E).

Here, small-necked blebs can be produced because, as the cortex contracts, it pulls on the adhesions and thereby retracts the cell membrane. This reduces the volume of the cell body. As the total volume is constant this means that a higher proportion of the volume is pushed into the bleb, causing it to be larger. The higher adhesion strength restricts the neck from increasing in size and, so, large blebs with small necks are produced.

Contracting the cortex also alters the relationship between extension and pressure. As we might expect, if we slowly squeeze the back of the cell (which is effectively what the cortical contraction is doing) the bleb can reach further whilst maintaining a higher pressure (dash-dot line in Fig. 6(c)). Unexpectedly, if we squeeze the back of the cell slightly quicker we initially cause the internal pressure to increase (dashed line in Fig. 6(c)). This in turn causes the bleb to grow quicker. As the bleb grows faster it reaches a point where membrane growth is unable to sustain subthreshold adhesions leading to unzipping of the neck width. Critically, the neck does not unzip completely and although the pressure does drop as the neck width increases it is not monotonic. This non-monotonic behaviour in the pressure stems from the neck growth undergoing a stick–slip phenomenon (Fig. 6(d)) (seen also in Appendix J) and is experimentally observed. Perhaps the most crucial observation is that squeezing the cell at two different speeds generates different sizes of bleb, both of which can be categorised as having small necks. Note that no tearing occurs unless the contraction is quick enough, offering a potential reason behind such phenomena and allowing us to separate different categories of blebs: those that undergo adhesion breaking and those that do not.

4. Summary and conclusion

We have modified a previously developed axisymmetric, elastic shell model for blebbing cells in order to include adhesion proteins. These adhesions couple the cell cortex and the cell membrane together and are modelled as linear springs that break if stretched too far. Critically, this simple framework did not reproduce the small-necked morphology that the blebs of stem cell muscles are observed to generate. Thus, the basic framework was extended in a number of different ways in order to study how small-necked-big blebs are created. By definition (Fig. 2), these are blebs whose maximum width is larger than the neck region from which they grew and whose extension is 1.5 μm, or larger. We focused on such blebs as it was believed that producing such a connecting neck with an acute angle between the cell and bleb would be difficult to sustain due to the large forces acting upon the adhesions.

It is possible that all of the extensions discussed in Section 3.2 and Appendices C–K have biological analogues as different cells display different blebbing characteristics (Maugis et al., 2010; Collins-Hooper et al., 2012). Moreover, it is possible that these mechanisms work in tandem in order to restrict the growth of the neck region. It is hoped that by demonstrating the difficulties surrounding the production of a small-necked bleb we will motivate experimentalists to clarify the main driving forces behind bleb formation. Equally, the large number of plausible mechanisms that give negative results adds to the evidence that blebs are highly controlled protrusions, rather than the random cellular extensions that they were initially thought to be.

Condensing our results, we see that the first prediction we produce is that small-neck-large blebs cannot be produced from simply altering the static structural properties of the membrane, or the adhesions. Explicitly, making the membrane stiffer, grow

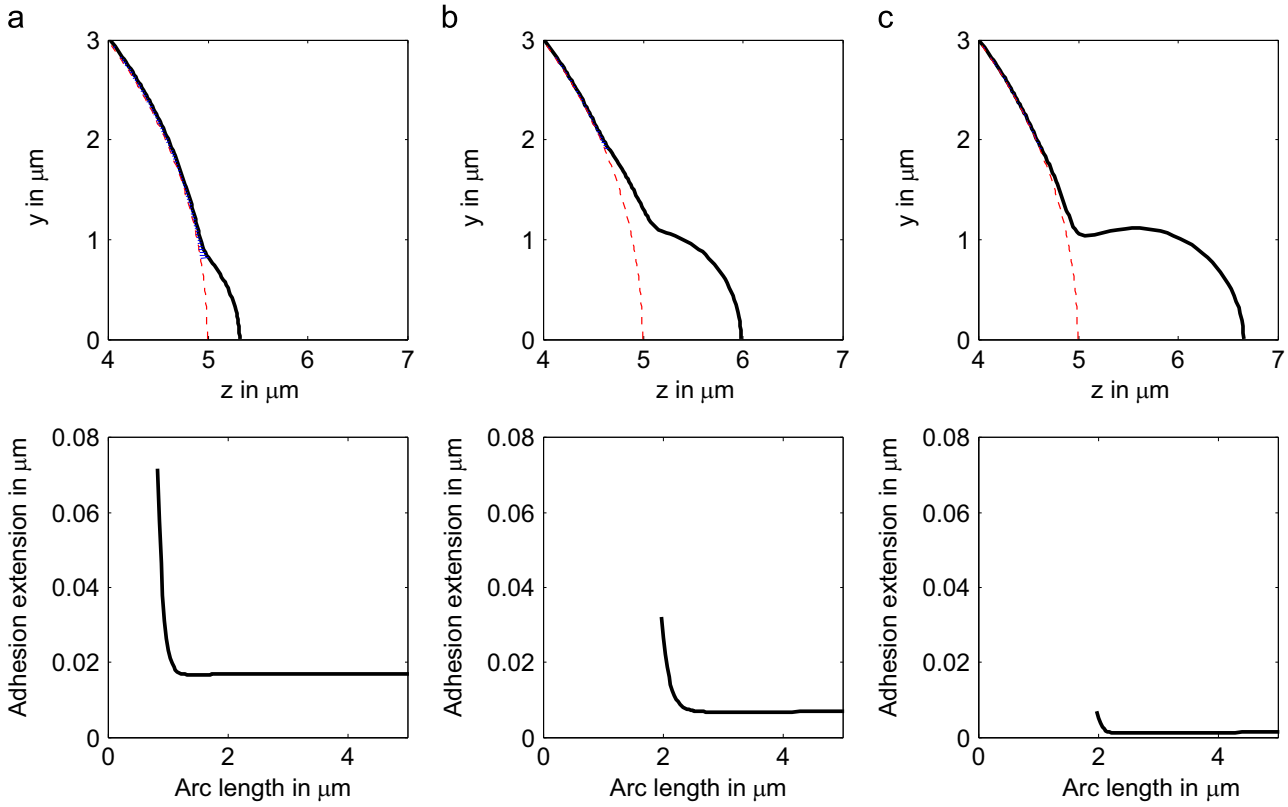

Fig. 5. Growth is localised to the region $\sigma \in [0, 1]$, μm whilst adhesions are allowed to break as normal. This is why the blue (unadhered) part of the membrane moves further along the arc length, whilst the bleb expansion remains local. Top row: cell profile. Bottom row: extension of adhesions. (a) Initialisation state. (b) The adhesions have stopped breaking and only growth is occurring. (c) The bleb is able to extend to experimentally observable sizes, whilst maintaining a small neck width. All other parameters and stages in the iteration are as in Fig. A1. (For interpretation of the references to colour in this figure caption, the reader is referred to the web version of this paper.)

faster, adhere more strongly, or altering other various adhesion properties does not produce the desired phenotype, although these extensions help reduce the amount of adhesion breaking to varying degrees.

Although they did not reproduce the small-necked-large-bleb morphology there are two particular base case perturbations that are worth mentioning. In particular, in Appendix J, we saw that a localised region of higher adhesions can reproduce the tear-slip membrane–cortex dynamics that are seen in experiments (Charras et al., 2008). However, the idea that blebs occur in regions of high adhesion patches is currently not supported in the biological literature. Equally, although our primary focus was on producing small-necked-big blebs, as seen on muscle stem cells, we have shown that increasing adhesion strength (Appendix I) can produce small-necked-small blebs, of the kind seen in amniotic stem cells. This suggests that the model can predict the differences between cell types and predict dominant mechanisms.

Having understood that the static intrinsic structural properties of our model cell do not give rise to the desired result we turned to alternative possible mechanisms that evolve over time. Critically, our next two mechanistic proposals, localised growth and cortex contraction, were successful in producing the small-necked profile of interest. Currently, experimental evidence supporting, or refuting, either mechanism is minimal. An immediate way to experimentally observe if local membrane growth occurs would be to put microdots on the membrane and visualise how the membrane moves during blebbing. If the microdots remain local in non-blebbing areas and move further apart on the bleb membrane, the hypothesis of local growth would be supported. Alternatively, it may be possible to use FRAP in order to see if membrane is recruited in blebs.

Currently, in support of the local growth hypothesis recent work has suggested that cells are able to deploy vast amount of aquaporin molecules specifically to blebbing sites (Patel and Dash, 2013). Aquaporins are proteins that control the water flow into, and out of, the cell by inserting themselves into the membrane. Further, when not in use, aquaporins are encapsulated in vesicles of extra membrane and stored within the cell (Takata et al., 2004). Not only does the existence of aquaporins suggest that we are unable to take volume conservation for granted, but they also offer a route providing the local membrane growth. As aquaporins have been observed to be completely localised to the blebs of a cell their deployment causes extra membrane from the vesicles to be added into localised regions, suggesting that local growth could initiate blebbing. Of course there is a question of cause and effect: is the addition of aquaporins the cause of the blebbing? Or are aquaporins added after the blebs form? This will be the subject of future work.

Equally, there is no evidence for, or against, muscle stem cells using global cortex contraction to produce blebs. The fact cell contraction that has not been reported in the literature may not be surprising as only a reduction of 10–50 nm in the cortex's radius is required to produce the effects shown in Section 3.2.2. This is the length scale of the adhesions and far below the wavelength of visible light and, thus, beyond the resolution of standard optical microscopy. Hence, unless the cortex's shrinking is investigated with super-resolution microscopy a contraction of this magnitude would not be observed. In support of cortex contraction driving blebbing it has been observed that if myosin motors, which create tension in the cortex, are inhibited then the number of blebs produced by a cell is reduced (Tinevez et al., 2009). Furthermore, other cell types, such as dictyostelium (Zatulovskiy et al., 2014),

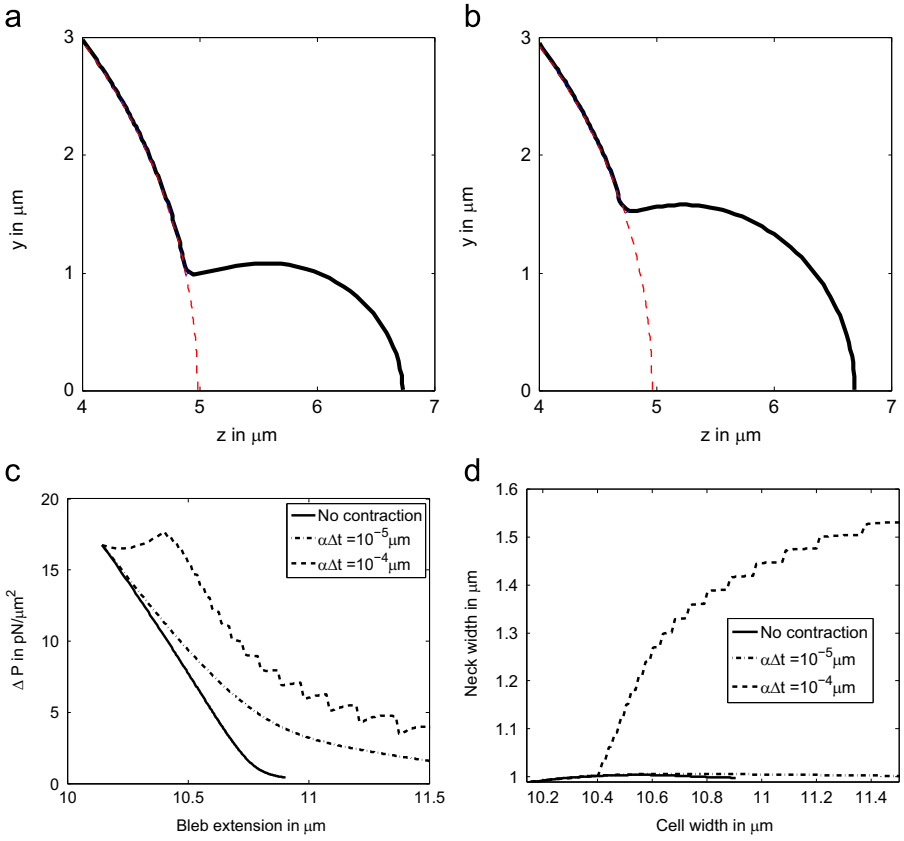

Fig. 6. Cortex contraction simulations. As the membrane grows the cortex is reduced in radius. This pulls on the adhesions connected to the membrane. The top row shows the protrusion profiles with varying values of contraction rate, $\alpha\Delta t$ (see Appendix K), whilst (c) illustrates the evolution of pressure as the bleb extends and (d) illustrates the balance between growth and reference reconfiguration. Parameters are (a) $\alpha\Delta t = 10^{-5}$ μm and (b) $\alpha\Delta t = 10^{-4}$ μm. In all cases $\kappa C = 4 \times 10^3$ pN/μm^3. All other parameters and stages in the iteration are as in Fig. A1.

are seen to have very active cortex dynamics which could easily account for the contraction needed to produce their blebs. However, although cortex tension is important it is not obvious that the cortex contracts upon bleb initiation in muscle stem cells. Using 10 nm as the order of magnitude value for contraction and assuming that the constitutive law, Eq. (12), is valid for the cortex then, since the cortex is close to a sphere, we can use Laplace's law to approximately work out the stiffness parameter for the cortex and therefore its Young's modulus by dividing the stiffness parameter by a typical cortex thickness, which is of the order 10^{-2} μm (Clark et al., 2013). From these figures we can estimate that Young's modulus of the cortex is 1 MPa, which is within typical estimates for biological materials (Ashby et al., 1995), although towards the lower end. This suggests that if the cortex were stiffer, it would not contract as much, from purely pressure driven means and, thus, this mechanism could not be supported. Note that other mechanisms may be actively remodelling the cortex, as can be seen in the extremely dynamic blebbing cells of Maugis et al. (2010).

Although simple our model has allowed us to test a number of current theories surrounding the production of blebs, with particular emphasis on protrusions that have neck widths smaller than the final protrusion's maximum width. We predict that combinations of cortex contraction and localised membrane growth are the most promising methods for generating small-neck-large blebs. Currently, neither proposed mechanism has been fully considered experimentally. Thus, we leave open conjectures concerning the mechanism underlying the formation of these blebs.

Acknowledgements

A.G. is a Wolfson Royal Society Merit Holder and acknowledges support from a Reintegration Grant under EC Framework VII PIRG6-GA-2009-256377. T.E.W. would like to thank St. John's College Oxford for its financial support.

Appendix A. Mathematical system

To close system (1)–(10) we need to specify constitutive relations, (12) and (13), that couple the surface tensions, t_s and t_ϕ, to the reference and solution configurations. Explicitly these are

$$t_s = A(\lambda_s^2 + \mu\lambda_\phi^2 - (1+\mu)), \tag{A.1}$$

$$t_\phi = A(\mu\lambda_s^2 + \lambda_\phi^2 - (1+\mu)). \tag{A.2}$$

Here we have appealed to large deformation theory to specify the constitutive law linking stresses and strains in the membrane. Further, we have assumed that the bending moments are isotropic and proportional to the mean surface curvature, i.e.

$$m_\phi = m_s = M(\kappa_s + \kappa_\phi - K_0), \tag{A.3}$$

where K_0 is the mean curvature of the reference configuration and M is the bending modulus.

A.1. Boundary conditions

We now derive the boundary conditions for system (1)–(10). We expand y, θ, s, t_s and λ_s in powers of σ near $\sigma = 0$ and in powers of $\pi\rho - \sigma$ near $\sigma = \pi\rho$. Here, we specify only the boundary conditions near $\sigma = 0$, with the conditions at $\sigma = \pi\rho$ being similar.

The expansions have the form

$$y = y_0 + \sigma y_1 + \sigma^2 y_2 + \ldots, \tag{A.4}$$

where the other variables are given *mutatus mutandis*. Since we are imposing that the z-axis is the axis of spherical symmetry the cell cuts the z-axis at the front, $z(0)$, and back, $z(\pi\rho)$, thus, we immediately fix $y_0 = \theta_0 = T_{s0} = Q_{s0} = Q_{s1} = s_0 = 0$. On expanding the equations near $\sigma = 0$ we find that

$$y_1 = \lambda_1, \tag{A.5}$$

$$\theta_1 = \kappa_{s0}\lambda_1, \tag{A.6}$$

$$s_1 = \lambda_1, \tag{A.7}$$

$$T_{s1} = \lambda_1 A\left(\lambda_1^2\left(\frac{1}{y_{rc1}^2} + \mu\right) - (1+\mu)\right), \tag{A.8}$$

where λ_1 satisfies the following quartic:

$$0 = \kappa_{s0}A\left(\frac{1}{y_{rc1}^2} + \mu\right)\lambda_1^4 - \frac{1}{2}(\Delta P + 2\kappa_{s0}A(1+\mu) - F(0)C(0))\lambda_1^2 + Q_{s2}^2, \tag{A.9}$$

with y_{rc} as the vertical coordinate of the reference configuration. In previous work (Woolley et al., 2014a,b) the consistency equation was a cubic polynomial. Here, the degree has increased because the equations are in terms of T_s and Q_s instead of t_s and q_s.

Eqs. (A.5) –(A.8) form the four boundary conditions needed to be satisfied at $\sigma = \epsilon \gg 1$. The final three come from deriving analogous equations at $\sigma = \pi\rho - \epsilon$ and noting that we do not need to specify two boundary conditions for the variable s. This is because, as discussed above, Eq. (4) decouples and can be solved as an initial value problem, once the rest of the system has been solved as a boundary value problem.

A.2. Update rule

To initialise the simulations adhesions are removed in the front of the cell, around $\sigma = 0$. After the initial ablation of adhesion the membrane deformation arises through reference configuration remodelling. This means that the arc length and profile of the reference configuration are able to update according to some postulated evolution rule. Critically, we only remodel the reference configuration within the unadhered region, $\sigma \in [0, \hat{\sigma}]$. Using the biologically demonstrated fact that strains are small (Nichol and Hutter, 1996), we fix the reference configuration update rule to be linear. Explicitly, if $y_{rc}(\Sigma, t)$ and $\Sigma = \Sigma(\sigma, t)$ are the profile of the reference configuration and corresponding arc length at time t, respectively, then

$$\frac{\partial y_{rc}}{\partial t}(\Sigma, t) = \eta_1(y(\Sigma, t) - y_{rc}(\Sigma, t)), \tag{A.10}$$

$$y_{rc}(\Sigma, 0) = \rho \sin(\sigma/\rho), \tag{A.11}$$

and

$$\frac{\partial \Sigma}{\partial t} = \eta_1(s - \Sigma), \tag{A.12}$$

$$\Sigma(\sigma, 0) = \sigma \in [0, \hat{\sigma}]. \tag{A.13}$$

Once the equilibrium state has been found y_{rc} and Σ are updated. These new values for the reference configuration and arc length are then substituted back into the equations and boundary conditions and the system is solved again.

A.3. Tearing enforcement

As the membrane position evolves the adhesions connecting it to the cortex may become stretched beyond an experimentally suggested critical length and break. This adhesion breaking is enforced through the adhesion concentration function, $C(\sigma)$. Initially, the

concentration of adhesions is uniform everywhere resulting in the membrane forming a spherical profile. $C(\sigma)$ is then defined in a piecewise constant manner over the intervals, $[0,\hat{\sigma})$ and $[\hat{\sigma},\pi\rho]$:

$$C(\sigma)=\begin{cases} c, & \sigma<\hat{\sigma},\\ C, & \sigma\geq\hat{\sigma}.\end{cases} \tag{A.14}$$

Over a number of solution iterations, which are used to initialise the model, c is reduced to zero, making $C(\sigma)$ a scaled Heaviside function, i.e. by the end of the model initialisation iterations there are no adhesions in the region $[0,\hat{\sigma})$, whereas $[\hat{\sigma},\pi\rho]$ is fully adhered. No remodelling of the membrane occurs within these first few simulation iterations. Thus, $[0,\hat{\sigma})$ is the ablated arc length, as illustrated in Fig. 2. The solution of system (1)–(10) under this piecewise adhesion condition provides an initial state and can be seen in Fig. A1. As mentioned previously, this initial state mimics the Tinevez et al. (2009) experiment of an instantaneous laser ablation of the cortex.

As the simulation progresses adhesion breaking is induced through the dependence of the adhesion concentration on $\hat{\sigma}$ (see Eq. (A.14)). The ablated arc length, $\hat{\sigma}$, is updated through the equation

$$\frac{\partial\hat{\sigma}}{\partial t}=\eta_2 H(E(\hat{\sigma})-E_c), \tag{A.15}$$

where $E(\hat{\sigma})$, calculated through Eq. (9), is the extension of the last remaining adhesion before the ablated region and E_c is the critical extension, taken to be 40 nm based on the estimates from the literature (Liu et al., 2007). The Heaviside function, H, ensures that the adhesions do not tear unless they are above the critical length, i.e. $E(\hat{\sigma})>E_c$.

A.4. Simulation process

Here, we discuss the simulation process as a whole and explicitly present the three steps that are completed over each adiabatic solution iteration. These three steps form the base case simulation against which all other results will be compared:

1. by using the pressure difference, ΔP, as a Lagrange multiplier system (1)–(10) is solved under the assumption of constant volume.
2. the adhesion break point, $\hat{\sigma}$, is updated, if necessary, as in Appendix A.3.
3. the reference configuration and arc length are updated through Eqs. (A.10) and (A.12) in the region in which adhesions are broken.

Each iteration is assumed to take exactly the same amount of time, Δt. Through knowing how many iterations are run, N, Δt is fixed by requiring that $N\Delta t=10$ s, which is a typical timescale for bleb expansion. This has been seen to give good qualitative and quantitative agreement with experimental velocity profiles of the membrane protrusions (Woolley et al., 2014a).

This general framework is used throughout all the simulations in Section 3. However, except for the base case simulation in Section 3.1, each simulation will be varied from this template in

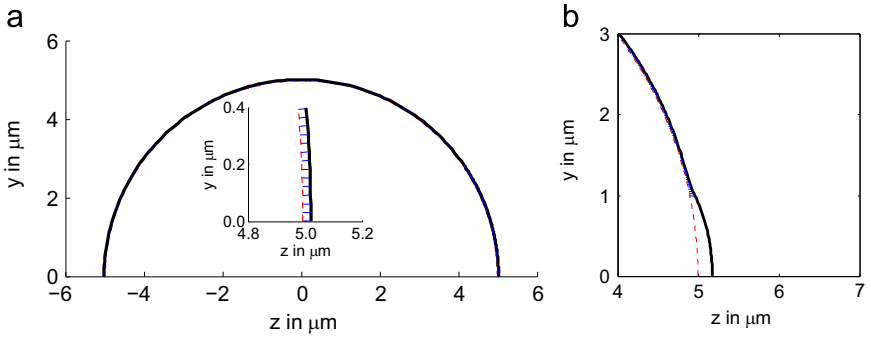

Fig. A1. Initialisation profile of the membrane. (a) Before the adhesions are ablated the solution is spherical. The inset shows a zoomed view of the right hand part of the cell. (b) Adhesions have been ablated along the arc length $\sigma\in[0,1]$ μm. Unless otherwise stated, the parameters used in this and all other simulations were 400 pN/μm, $M=10^{-2}$ pN μm, E_c=40nm, $\eta_1\Delta t=0.5$, $\eta_2\Delta t=0.03$ μm and $\kappa C=10^3$ pN/μm^3. Initially $\Delta P=$ 20 pN/μm^2 and $\hat{\sigma}=1$ μm.

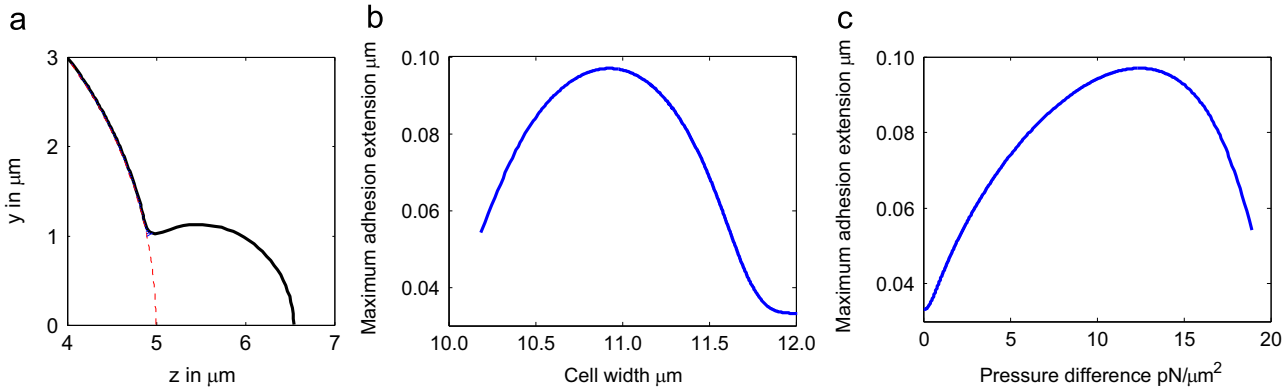

Fig. B1. Adhesions modelled as linear springs that do not break outside of the initial ablated arc length. (a) Cell profile. (b) Relationship between the maximum adhesion extension and cell width. (c) Relationship between the maximum adhesion extension and the pressure difference. All other parameters and stages in the iteration are as in the base case, Fig. A1.

order to investigate how we may best form blebs with a small neck width. These variations will be clearly discussed as appropriate.

Appendix B. No adhesion peeling

Here, we first present the system in the absence of adhesion breaking. This simulation illustrates the problems of maintaining small-necked-big blebs in the face of adhesion ablation. This first simulation is unphysical, in that after the system is initialised and the adhesions are ablated from $\sigma \in [0, \hat{\sigma})$ no more adhesions are allowed to break. Instead, the adhesions are allowed to stretch to any length they are able to reach. Essentially, we have set $\eta_2 = 0$ in (A.15). Although unphysical, it is useful to see the maximum adhesion extension and, hence, by how far the adhesion critical length, E_c, is violated.

As can be seen from Fig. B1(a), by not allowing the membrane to peel back away from the cortex the cell is able to support the production of small-necked blebs. This is because as the bleb grows the neck width is fixed. However, the maximum adhesion extension achieved is well over twice the expected value (adhesion lengths of this size are never seen (Liu et al., 2007), even though by the end of the simulated expansion all adhesions are, once again, below the critical length (see Fig B1(b)). This occurs because as the bleb extends the pressure decreases until, finally, the adhered membrane effectively collapses onto the cortex. This is observed in Fig. B1(c), where we see the pressure has to be less than 1 pN/μm^2 before the adhesions are once again all below the critical threshold of $E_c = 0.04$ μm.

Appendix C. Altering μ

As the parameter μ controls the shell's stiffness ratio between the arc length and azimuthal directions, simulations were run to see if altering this ratio would significantly influence neck size. The idea being that by altering this ratio it would be easier to extend the bleb axially, rather than azimuthally, whence a small neck may have been feasible.

Simulations in Fig. C1 demonstrate that, although it is slightly better to have a smaller value of μ, neither extremely high values ($\mu = 0.9$) or low values ($\mu = 0.1$) of μ greatly influenced the profiles. This corroborates the findings of Woolley et al. (2014a), where it was noticed that the model was fairly insensitive to changes in μ.

Appendix D. Time scale

One key point to notice about the base case simulation is that remodelling occurs on the same time scale as the adhesion breaking. Explicitly, during a single iteration there is one membrane reconfiguration step and one adhesion breaking step. Here, we investigate the effect of pushing these time scales to the extreme favour of either the adhesion breaking or the reference reconfiguration.

Firstly, we assume that adhesion breaking occurs on a much faster time scale than membrane growth, thus, growth will only occur once no adhesions are above the critical length. If any adhesions extend beyond the critical length during the reconfiguration process growth is halted and adhesion breaking is once again enforced until all remaining adhesions fall below the critical length.

As we may have expected the neck width in the faster tearing simulation (Fig. D1(a)) is significantly larger than the base case's neck width of approximately 2 μm (Fig. 4(c)). Without membrane growth the bleb is unable to extend and cause the pressure difference to drop, which in turn relieves the tension in the springs. The only way to relieve tension in the adhesions is for them to break. Hence, membrane peeling will continue to occur until the pressure difference is small enough to allow all adhesions to fall below their critical length. Then, and only then, can the membrane start growing. However, once the tearing stops the pressure difference acting on the membrane is so small that the difference between the solution and reference states is extremely small. As the reconfiguration process is proportional to this difference, reconfiguration (and therefore bleb extension) is essentially halted. Over all, this means that protrusions cannot extend much beyond 0.5 μm, whereas the base case saw a protrusion of over 1 μm (see Fig. 4(c)).

Secondly, we increased the speed of reconfiguration of the reference configuration: it was updated instantaneously. This means that within the unadhered zone the reference configuration is updated to the solution configuration exactly. This increases the amount of membrane added to the reference configuration after each iteration.

We expect that faster membrane reconfiguration will decrease the neck size because faster reconfiguration will cause the

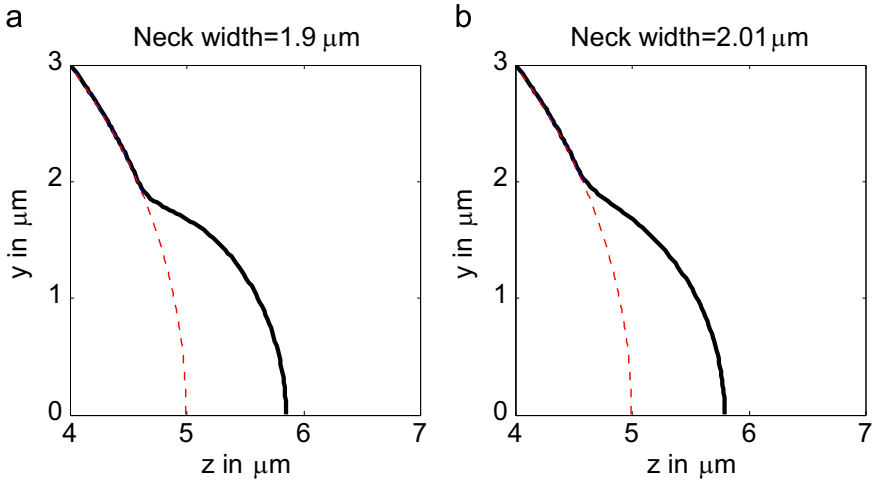

Fig. C1. Varying the value of μ, (a) $\mu = 0.1$ and (b) $\mu = 0.9$. All other parameters and stages in the iteration are as in Fig. A1.

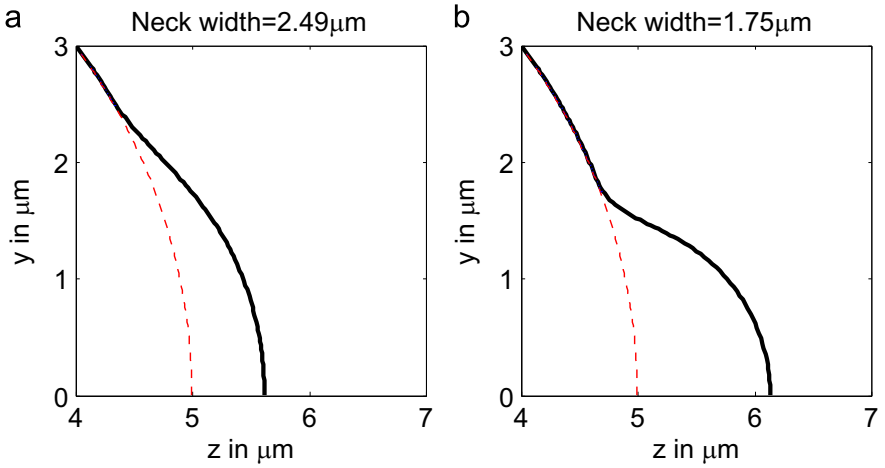

Fig. D1. Changing adhesion breaking and membrane growth time scales. (a) Any adhesions above the critical length are broken and the geometry is allowed to update. These two stages of breaking and geometry updating are iterated until no adhesions are above the critical length. Remodelling is then allowed to occur. (b) Remodelling is instantaneous, in that the reference configuration for the next solution is fixed to be the current solution configuration. All other parameters and stages in the iteration are as in Fig. A1.

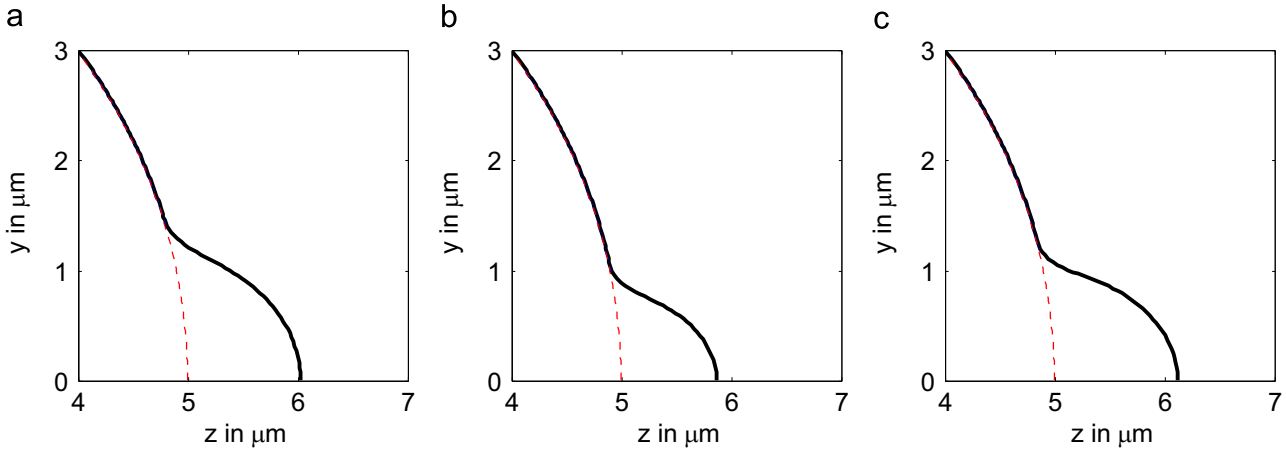

Fig. E1. Profiles simulated with increased adhesion strength density and pressure difference. All three simulations have been run for the same number of iterations. The adhesion strength densities and initial pressure differences are (a) $\kappa C = 2 \times 10^3$ pN/μm^3 and $\Delta P = 20$ pN/μm^2; (b) $\kappa C = 5 \times 10^3$ pN/μm^3 and $\Delta P = 20$ pN/μm^2; (c) $\kappa C = 5 \times 10^3$ pN/μm^3 and $\Delta P = 40$ pN/μm^2. All other parameters and stages in the iteration are as in Fig. A1.

reference configuration's volume to become larger faster. This increase in reference configuration volume causes the pressure difference, ΔP, to drop. Consequently the adhesions reduce in size and, hence, adhesion breaking stops earlier. Fig. D1(b) confirms this is the case as the neck width in the faster remodelling case is smaller that the base case's neck width (Fig. 4(c)). However, it does not stabilise a neck smaller than the maximum bleb width.

If the ratio of adhesion breaking rate to membrane growth rate was pushed further towards increasing the reconfiguration time scale (for example, by reducing the adhesion breaking rate) we would eventually arrive at the simulations in Appendix B. Namely no adhesions would break and small neck blebs would be possible. Altogether, Fig. D1 suggests that within our current model membrane growth must be as fast, if not much faster, than adhesion breaking in order for small-necked blebs to form.

Appendix E. Higher adhesion strength density

Perhaps one of the easiest methods of creating a smaller neck width is by increasing the force needed to separate membrane and cortex. This can be achieved either by increasing the adhesion density, C, or by increasing the spring constant, κ, of the adhesions. In either case it is the adhesion strength density, κC, which is the parameter grouping of interest. Note that although κC is increased in this section, similar to the base case, the system is initiated by totally removing the adhesions within the ablated region $[0, \hat{\sigma}]$. Thus, at the point the solution iterations are begun κC is, once again, a scaled Heaviside function, as in Eq. (A.14).

Fig. E1 immediately shows that the adhesion strength density greatly influences the protrusion profile. Primarily, Fig. E1 (a) illustrates that just a doubling of the base case adhesion strength density is enough to reduce the neck width of the protrusion from 2 μm to 1.4 μm, although peeling still occurs. Increasing the base case κC five-fold allows protrusions to be created, without tearing occurring at all (Fig. E1(b)).

Unfortunately, for the same initial pressure difference as in the base case, $\Delta P = 20$ pN/μm^2, the protrusions do not extend far enough to produce a small-necked-big bleb. This occurs because, for the same pressure difference, increasing the adhesion strength density causes the initial volume of the shell model to be smaller. Because volume is conserved throughout the simulation this means that less volume can be transported into the expanding region, resulting in miniature blebs.

The influence of the adhesion strength density on the cell radius can be derived analytically from system (1)–(10). Before adhesions are ablated, all parameters are constant over the entire cell. This causes the initial equilibrium solution to be spherical. Using this knowledge we can simplify the governing equations to

$$t_s = A\left(\left(\frac{r}{\rho}\right)^2 - 1\right)(1+\mu), \tag{E.1}$$

$$\frac{2t_s}{r} = \Delta P - FC, \tag{E.2}$$

$$F = \kappa(r-\rho). \tag{E.3}$$

Using the fact that $r \approx \rho$ we can linearise system (E.1)–(E.3), allowing us to derive a higher order correction for r, namely

$$r \approx \rho\left(1 + \frac{\rho\Delta P}{4A(1+\mu)+\kappa C\rho^2}\right), \tag{E.4}$$

which clearly illustrates the approximate functional relationship that the radius has with the adhesion force density, κC. Eq. (E.4) suggests that the problem of decreasing radius with increasing κC can be counteracted by increasing the initial pressure difference, ΔP. We also note that reducing A will hardly change the radius as the denominator will be dominated by the $\kappa C\rho^2$ term.

Although we see that increasing the pressure difference will aid in increasing the volume of the cell we are physically bounded by what values the pressure difference can realistically take. Dai and Sheetz (1999) suggest that pressure difference is approximately 20–30 pN/μm^2, which is the range we are considering. Furthermore, we need to balance the adhesion force and pressure difference, because if the pressure is increased then the adhesions will, once again, start to break, making the membrane peel back. In particular, this balancing problem makes it very difficult to produce small-necked blebs, see Fig. E1(c). Since not all blebs have small necks a cell's balance between pressure and adhesion strength is an important factor in dictating the final size and shape of a bleb. This is a crucial point since there is still a problem of the final pressure difference in equilibrium states (visualised in Fig. E1) being much smaller than the initial value, making capturing multiple blebs within a mechanical modelling framework a difficult problem.

Appendix F. Stochastic adhesion profile

Although the adhesion strength density, κC, is treated as a piecewise constant this is an over simplification of the adhesion molecule distribution. As such, in this section we alter the method to include a stochastic adhesion strength density profile. Namely, a randomised profile

$$\kappa C(\sigma) = \begin{cases} 0, & \sigma < \hat{\sigma} \\ |\overline{\kappa C} + \eta(\sigma)|, & \sigma \geq \hat{\sigma} \end{cases}, \tag{F.1}$$

is generated at the beginning of the simulation and then fixed throughout. The variable η is sampled from a normally distributed random variable with mean zero and variance ν. Fixing $\overline{\kappa C} = 10^3$ pN/μm^3 and varying ν over the values 1, 10 and 1000 we found that a randomised profile had very little effect on the final profiles of the simulations and offered no benefit over the base case in terms of producing a small-neck-large-bleb protrusion (results not shown). From these simulations we feel confident in the knowledge that, although the distribution of adhesion molecules and their strength may not be uniformly constant over the surface of the cell, small variations do not influence the underlying results.

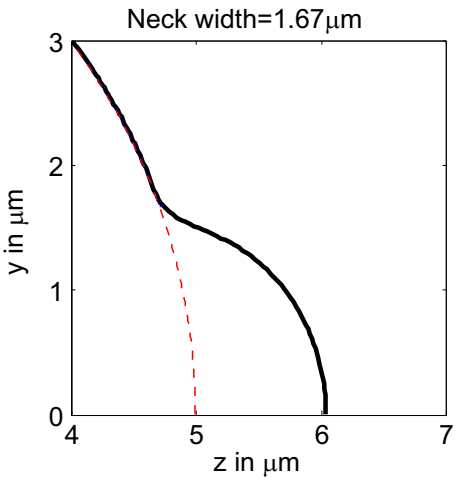

Fig. G1. Adhesions follow a quadratic relationship between the applied force and extension. All other parameters and stages in the iteration are as in Fig. A1.

In contrast, stochasticity in the adhesion strength density may offer an initiating mechanism for blebbing. It has been suggested that blebs simply expand from sites where adhesions are momentarily weaker. The weaker sites arise purely through stochastic fluctuations in the adhesion populations.

Appendix G. Non-linear adhesions

Another potential way of reducing the arc length over which adhesions break is to change the force–extension curve that the springs obey. Previously, the adhesions have been modelled as Hookean springs, meaning that their force–extension relation has been linear until breaking point. Here, we suppose that the adhesions act like catch bonds (Dembo et al., 1988) and become stiffer as they are stretched, although they still break once they are stretched beyond 40 nm. The quadratic form of the force is

$$F = \frac{\kappa}{\beta}(r-\rho)^2, \tag{G.1}$$

where β is chosen such that the initial spherical solution radius of the fully adhered system is the same as the radius in the linear spring case. In order to ensure this equality the linear and quadratic force values must be the same as the initial separation. Therefore, β must be equal to the initial separation of the cortex and membrane, $r-\rho$. Considering Eqs. (E.1)–(E.3) we deduce that

$$\beta = \frac{\rho^2\Delta P}{4A(1+\mu)+\kappa C\rho^2}. \tag{G.2}$$

This idea can be compared to that of having a higher adhesion strength density, as in Appendix E. In particular, the non-linear adhesions have the same benefits that arise with the higher adhesion strength density cases, whilst not having the same drawbacks. One such benefit is that the non-linear adhesions only dominate the pressure/adhesion force balance once the adhesions begin to stretch. This means that the initial equilibrium state will have a larger volume than if the adhesions were simply strengthened everywhere all the time (as in Appendix E). A second benefit stems from the fact that we need not assume that the non-linear adhesions are a local effect, as in the case of the higher adhesion neck ring, see Appendix J.

As shown in Fig. G1 simulations suggest that the cell's response to this change is unable to reproduce the desired effects. Explicitly, the protrusion's neck does not peel as far back as the base case,

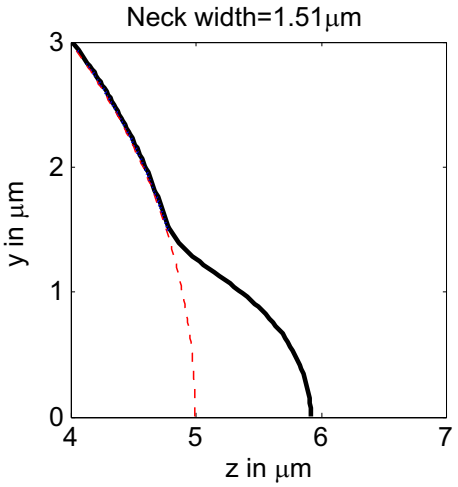

Fig. H1. Adhesions are connected normally to the membrane, thus the red spring illustrate the membrane's normal directions. All other parameters and stages in the iteration are as in Fig. A1. (For interpretation of the references to colour in this figure caption, the reader is referred to the web version of this paper.)

however, the neck is still not small enough for protrusions to be small-necked blebs.

Appendix H. Normal adhesion force

From the derivation illustrated in Fig. 3 the springs, which model the adhesion proteins, are assumed to be constantly connected to the points at which they were originally fixed. In other words, the springs are fixed in both cortex and membrane and only move due to the changes in the geometry that arise from membrane growth. There is some evidence to suggest that ezrin could be fixed in the membrane in this way and thereby allow the membrane to undergo shear forces (Liu et al., 2007; Treanor et al., 2010). However, the predominant thought is that, although ezrin should be fixed in the cortex, the membrane is a more fluid structure (Gennis, 1989) and, hence, the adhesions will act normally to the membrane.

This alternative is simple to implement as we calculate the normal angle θ as part of the solution. From this we fix $\delta=\theta$ and calculate the point at which the normal line hits the cortex and thereby calculate the adhesion extension.

Similar to the stochastic description of adhesion density this perturbation to the base case offers hardly any benefits with respect to neck and bleb size. Fig. H1 demonstrates clearly that the membrane does not peel as far in the base case, but the protrusions are still unable to maintain small necks. Essentially, the adhesions are too small for the adhesion angle to make a large difference.

Appendix I. Smaller neck size initiation

We examine the influence of the initial adhesion ablation arc length, $\hat{\sigma}_0$, on the neck width of the bleb. We postulate that if a smaller region of adhesions is initially ablated the bleb may be able to grow without the excessive tearing that occurs when a large region of adhesion is ablated. Hence, reducing the region of initial ablation may lead to blebs with smaller necks.

Note that, although as the adhesive strength is increased larger ablated arc lengths can be stabilised, this does not mean that we can increase the ablated region and expect small-neck-large-bleb profiles. Increasing the adhesion strength density not only stops membrane–cortex tearing it also reduces the potential size of the expansion, as discussed in Appendices E and J. Therefore it is only possible to produce small blebs under the mechanism of increasing adhesion strength density.

Fig. I1(a) shows that if the initial ablation region is below $\hat{\sigma}=0.2\,\mu$m, when $\kappa C=1\times10^3$ pN/μm^3, or if it is below $\hat{\sigma}=0.4\,\mu$m, when $\kappa C=3\times10^3$ pN/μm^3, then adhesion breaking does not occur. Hence, as the adhesion strength density increases so does the ablation arc length over which tearing does not occur.

By plotting the initial ablation size against the final neck width not only do we see a critical peeling threshold for the ablation length, but we also notice a sharp transition between peeling and non-peeling schema. This sharp transition can also been seen in the $\kappa C=1\times10^3$ pN/μm^3 case when we consider the relationship between the initial ablated arc length and the cell's width (see Fig. I1(b)). This can be compared with the $\kappa C=3\times10^3$ pN/μm^3 case, which has a smoother connection through the bifurcation point of approximately $\hat{\sigma}=0.4\,\mu$m. This means that, unlike the $\kappa C=1\times10^3$ pN/μm^3 case, small rounded profile protrusions can arise in the $\kappa C=3\times10^3$ pN/μm^3 case since the cell width is able to increase further before adhesion breaking occurs. The profiles of such protrusions can be seen in Fig. I1(b), from which we observe that although the blebs are less than 1 μm in extension, the bleb's maximum width is larger than their neck width, thus, these protrusions are 'small-necked-small blebs'. Although these are not the phenotype present in muscle stem cells, we suggest that they are similar to the smaller blebs present in amniotic cells, which are also used for migration.

Appendix J. Adhesion ring

In Appendix E the adhesion strength density was increased homogeneously. However, adhesions need not be strengthened everywhere. By increasing the adhesion strength density only in a small region around the blebbing membrane the bleb neck can be maintained, whilst peeling is stopped completely, as seen in Appendix J. This occurs because, for a given initial pressure, the adhesion ring simulations will have a higher initial volume constant, when compared to the uniformly increased adhesion strength density, hence, more of this volume can be transported into the blebbing region, thereby creating larger blebs.

We firstly note that, upon application of the adhesion ring, the spherical solution is no longer valid in the fully adhered case, because the equations are no longer spherically symmetric. Explicitly, the membrane near $\sigma=0$ is pulled in closer to the cortex due to the localised higher adhesion strength density. This effect is subtle, but visible in the inset of Fig. J1(a), as well as in the adhesion extension plot.

Once the adhesions have been ablated we see from the adhesion extension plot in Fig. J1(b) that all remaining adhesions are below critical length E_c=40 nm, thus, at least for the first few iterations, adhesion breaking does not occur and bleb growth is through membrane reconfiguration only. As the protrusion extends the adhesions become stretched, leading to some of the membrane tearing away from the cortex. Even after adhesion breaking has ceased occurring, the final neck width is below the base case value, Fig. J1(c), and the simulation is able to support a big bleb in which its neck is approximately the same as the bleb width.

Note that, due to the membrane having small, but non-zero bending, the membrane overshoots the equilibrium length of the adhesions in Fig. J1(c). In previous solutions all adhesions were larger than their equilibrium length and, so, were pulling the membrane and cortex closer together. In this case the adhesions

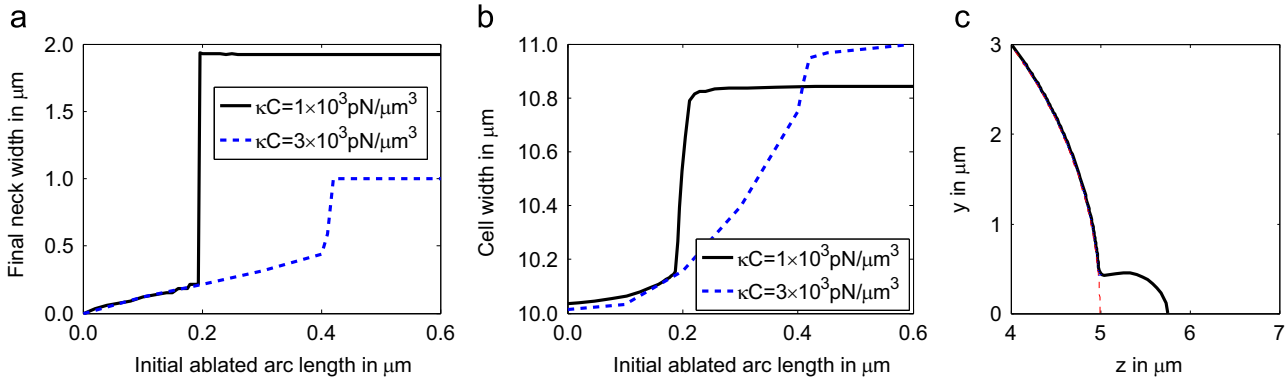

Fig. I1. Varying the size of the arc length over which adhesions are initially ablated. (a) The relationship between the ablated arc length and neck width. (b) The relationship between the ablated arc length and cell width. (c) A small-necked-small-bleb profile. $\kappa C = 3 \times 10^3$ pN/μm^3. All other parameters and stages in the iteration are as in Fig. A1.

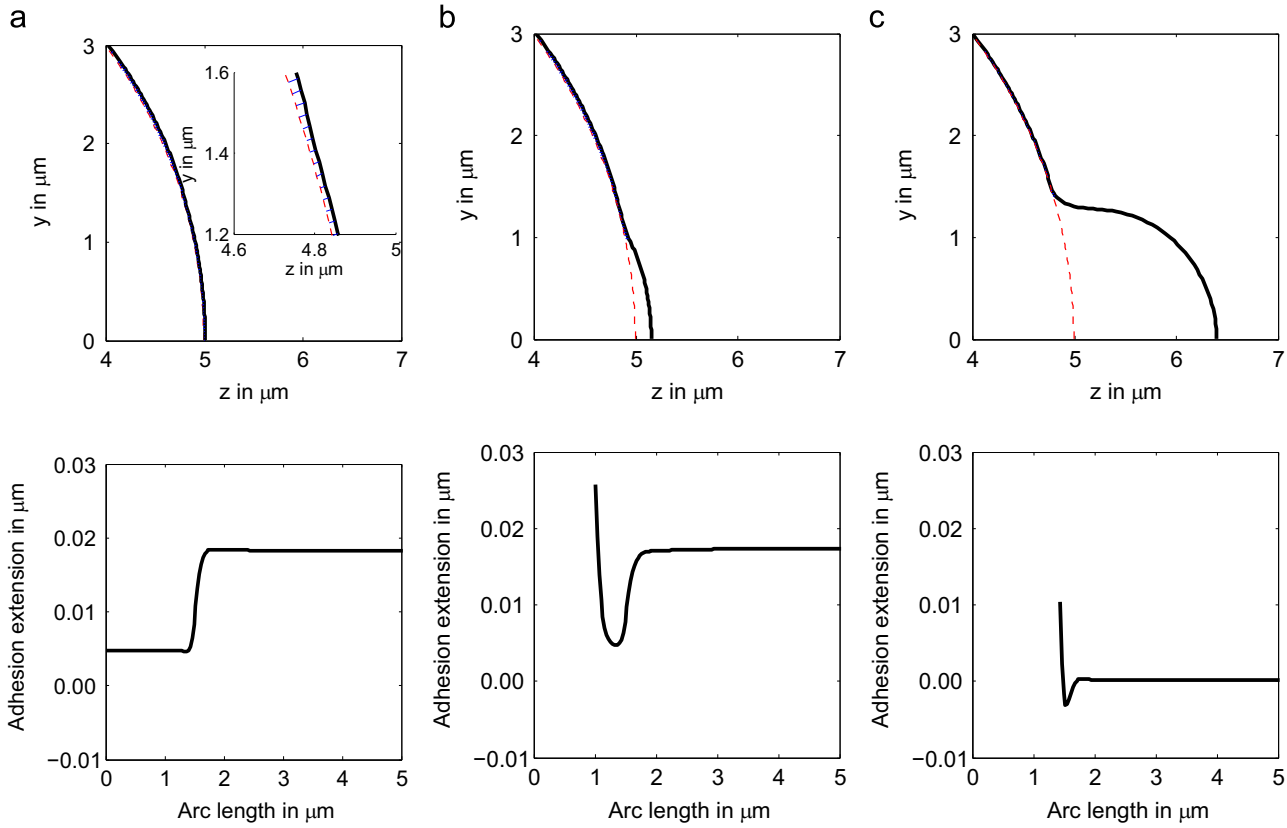

Fig. J1. Higher adhesion strength applied to a local vicinity around the bleb. Top row: cell profiles during the simulation. Bottom row: adhesion extension over the reference configuration's arc length. (a) Initial state profile before ablation or growth occurs. The inset shows a zoomed in section of the cortex, adhesion and membrane configuration near the transition point, $\sigma = 1.5$, where adhesion strength density is increased. The subtle effect of the membrane being pulled closed to the cortex due to the higher adhesion strength density region can be best seen in the adhesion extension graph. (b) Cell profile and adhesion extension immediately after ablation. (c) Final state of the cell. Initially, $\kappa C = 4 \times 10^3$ pN/μm^3 for $\sigma \in [0, 1.5]$ and $\kappa C = 1 \times 10^3$ pN/μm^3 elsewhere. All other parameters and stages in the iteration are as in Fig. A1.

around the neck of the bleb are actually pushing the cortex and membrane further apart.

Unlike previous simulations tearing does not start immediately, rather it occurs because of membrane growth. Moreover, the increased adhesion collar gives the system an emergent feature that once tearing starts, it is not continuous. In this case the mechanism is of a stick–slip variety. Explicitly, after a small number of adhesions breaking the lengths of all other adhesions fall below the critical length and, hence, adhesion break halts. The simulations continue reconfiguring the reference profile, without adhesion breaking, until a solution is reached in which adhesions are once again above the critical length. This can be seen in Fig. J2.

Effectively, we can think of an increase in cell width being due to membrane growth, whilst an increase in neck size is due to adhesion breaking. In the base case we see that the effect of each mechanism is of the same order. This can be compared with the adhesion ring simulation. Not only does the simulation reconfigure the membrane more than it breaks adhesions, but the jagged, stair-like increase illustrates the stick–slip phenomena.

In summary, although we have the potential to create small-necked-big blebs, a pertinent criticism of this approach is that we are artificially increasing the adhesion strength within a given region around the bleb. Whilst there is some stochastic variation within the adhesion concentration (see Appendix F), no experimental evidence

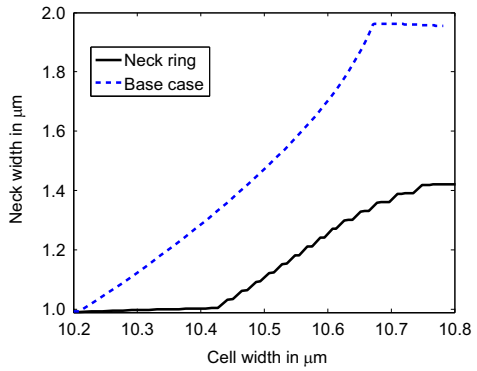

Fig. J2. Comparing how the neck and width of the cell grows in both the base call and the adhesive neck ring simulations.

suggests that the adhesion concentration is consistently larger around the neck region of a bleb. Moreover, the only evidence for heterogeneity in adhesion density (other than stochastic variations) suggests that it is actually the non-blebbing side that contains more adhesions (Lorentzen et al., 2011). Equally, increasing the adhesion strength in a local area does not account for the laser ablation experiments (Tinevez et al., 2009) that initiate the formation of a bleb at a random point on the cell.

Appendix K. Cortex contraction

Cortex contraction is simulated by reducing the cortex radius by a constant, small amount, α, after each iteration. The reason we choose to reduce the radius by a constant amount each time is because its reduction is extremely small, as discussed in Section 4. Algebraically, this is

$$\frac{\partial r_c}{\partial t} = -\alpha, \tag{K.1}$$

and applied through the discretisation

$$r_c(t+\Delta t) = r_c(t) - \alpha \Delta t, \tag{K.2}$$

where $\Delta t \alpha \ll 1$. The value of $\alpha \Delta t$ is chosen to fit the number of iterations over which the cell evolves. Because we have no data on this parameter we vary it over simulations and observe the solution's dependence on the rate of contraction. One thing is clear though: the total contraction over the simulation must be small as it has not been experimentally observed. Explicitly, the contraction should be on the order of nanometres, which is below the resolution of current confocal microscopy.

Alternatively, if the pressure from the cytosol acts on the actin skeleton as well as the membrane then, instead of the cortex contraction being an active process, cortex contraction could occur passively due to the bleb expansion reducing the pressure, which, in turn, would cause the actin skeleton to contract. In either case, because the rate of change is so small we choose to approximate the cortex contraction through a linear decrease in radius, which allows us to investigate the influence of the contraction time scale, as seen in Section 3.2.2.

References

Ashby, M.F., Gibson L.J., Wegst, U., Olive, R. 1995. The mechanical properties of natural materials. I. Material property charts. Proc. R. Soc. A 450 (1938), 123–140.

Bretscher, A., Reczek, D., Berryman, M., 1997. Ezrin: a protein requiring conformational activation to link microfilaments to the plasma membrane in the assembly of cell surface structures. J. Cell Sci. 110 (24), 3011–3018.

Charras, G., Paluch, E., 2008. Blebs lead the way: how to migrate without lamellipodia. Nat. Rev. Mol. Cell Biol. 9 (9), 730–736.

Charras, G.T., 2008. A short history of blebbing. J. Microsc. 231 (3), 466–478.

Charras, G.T., Coughlin, M., Mitchison, T.J., Mahadevan, L., 2008. Life and times of a cellular bleb. Biophys. J. 94 (5), 1836–1853.

Clark, A.G., Dierkes, K., Paluch, E.K., 2013. Monitoring actin cortex thickness in live cells. Biophys. J. 105 (3), 570–580.

Collins-Hooper, H., Woolley, T.E., Dyson, L., Patel, A., Potter, P., Baker, R.E., Gaffney, E.A., Maini, P.K., Dash, P.R., Patel, K., 2012. Age-related changes in speed and mechanism of adult skeletal muscle stem cell migration. Stem Cells 30 (6), 1182–1195.

Cunningham, C.C., 1995. Actin polymerization and intracellular solvent flow in cell surface blebbing. J. Cell Biol. 129 (6), 1589–1599.

Dai, J., Sheetz, M.P., 1999. Membrane tether formation from blebbing cells. Biophys. J. 77 (6), 3363–3370.

Dembo, M., Torney, D.C., Saxman, K., Hammer, D. 1988. The reaction-limited kinetics of membrane-to-surface adhesion and detachment. Proc. R. Soc. B 234 (1274), 55–83.

Evans, E.A., Skalak, R., 1980. Mechanics and Thermodynamics of Biomembranes. CRC Press, Boca Raton Florida.

Folkman, J., Moscona, A., 1978. Role of cell shape in growth control. Nature 273 (5661), 345–349.

Gennis, R.B., 1989. Biomembranes: Molecular Structure and Function. Springer-Verlag, New York.

Hu, J., 2009. Mathematical Modeling and Analysis of in vitro Actin Filament Dynamics and Cell Blebbing (Ph.D. thesis), University of Minnesota.

Köppen, Mathias, Fernández, B.G., Carvalho, L., Jacinto, A., Heisenberg, C.-P., 2006. Coordinated cell-shape changes control epithelial movement in zebrafish and Drosophila. Development 133 (14), 2671–2681.

Liu, D., Ge, L., Wang, F., Takahashi, H., Wang, D., Guo, Z., Yoshimura, S.H., Ward, T., Ding, X., Takeyasu, K., Yao, X., 2007. Single-molecule detection of phosphorylation-induced plasticity changes during ezrin activation. FEBS Lett. 581 (18), 3563–3571.

Lorentzen, A., Bamber, J., Sadok, A., Elson-Schwab, I., Marshall, C.J., 2011. An ezrin-rich, rigid uropod-like structure directs movement of amoeboid blebbing cells. J. Cell Sci. 124 (8), 1256–1267.

Maugis, B., Brugués, J., Nassoy, P., Guillen, N., Sens, P., Amblard, F., 2010. Dynamic instability of the intracellular pressure drives bleb-based motility. J. Cell Sci. 123 (22), 3884–3892.

Nichol, J.A., Hutter, O.F., 1996. Tensile strength and dilatational elasticity of giant sarcolemmal vesicles shed from rabbit muscle. J. Phys. 493, 187.

Otto, A., Collins-Hooper, H., Patel, A., Dash, P.R., Patel, K., 2011. Adult skeletal muscle stem cell migration is mediated by a blebbing/amoeboid mechanism. Rejuvenation Res. 14 (3), 249–260.

Patel, K., Dash, P.R., 2013. Personal communication.

Phillips, H.M., Rhee, H.J., Murdoch, J.N., Hildreth, V., Peat, J.D., Anderson, R.H., Copp, A.J., Chaudhry, B., Henderson, D.J., 2007. Disruption of planar cell polarity signaling results in congenital heart defects and cardiomyopathy attributable to early cardiomyocyte disorganization. Circ. Res. 101 (2), 137–145.

Pozrikidis, C., 2001. Effect of membrane bending stiffness on the deformation of capsules in simple shear flow. J. Fluids Mech. 440, 269–291.

Sahai, E., Marshall, C.J., 2003. Differing modes of tumour cell invasion have distinct requirements for Rho/ROCK signalling and extracellular proteolysis. Nat. Cell. Biol. 5 (8), 711–719.

Sheetz, M.P., Sable, J.E., Döbereiner, H.G., 2006. Continuous membrane-cytoskeleton adhesion requires continuous accommodation to lipid and cytoskeleton dynamics. Annu. Rev. Biophys. Biomol. Struct. 35, 417–434.

Singhvi, R., Kumar, A., Lopez, G.P., Stephanopoulos, G.N., Wang, D., Whitesides, G.M., Ingber, D.E., 1994. Engineering cell shape and function. Science 264 (5159), 696–698.

Strychalski, W., Guy, R.D., 2012. A computational model of bleb formation. Math. Med. Biol. 12 (2), 462.

Takata, K., Tajika, Y., Matsuzaki, T., Aoki, T., Suzuki, T., Abduxukur, A., Hagiwara, H., 2004. Molecular mechanisms and drug development in aquaporin water channel diseases: water channel aquaporin-2 of kidney collecting duct cells. J. Pharmacol. Sci. 96 (3), 255–259.

Tinevez, J.Y., Schulze, U., Salbreux, G., Roensch, J., Joanny, J.F., Paluch, E. 2009. Role of cortical tension in bleb growth. Proc. Nat. Acad. Sci. 106 (44), 18581–18586.

Tozluoğlu, M., Tournier, A.L., Jenkins, R.P., Hooper, S., Bates, P.A., Sahai, E., 2013. Matrix geometry determines optimal cancer cell migration strategy and modulates response to interventions. Nat. Cell. Biol. 15, 751–762.

Treanor, B., Depoil, D., Gonzalez-Granja, A., Barral, P., Weber, M., Dushek, O., Bruckbauer, A., Batista, F.D., 2010. The membrane skeleton controls diffusion dynamics and signaling through the B cell receptor. Immunity 32 (2), 187–199.

Tsukita, S., Yonemura, S., Tsukita, S., 1997. ERM (ezrin/radixin/moesin) family: from cytoskeleton to signal transduction. Curr. Opin. Cell. Biol. 9 (1), 70–75.

Woolley, T.E., Gaffney, E.A., Oliver, J.M., Baker, R.E., Waters, S.L., Goriely, A., 2014a. Cellular blebs: pressure-driven, axisymmetric, membrane protrusions. Biomech. Model. Mech. 13 (2), 463–476.

Woolley, T.E., Gaffney E.A., Waters S.L., Oliver J.M., Baker R.E., Goriely A., 2014b. Three mechanical models for blebbing and multi-blebbing. IMA J. App. Math. 79 (4), 636–660.

Zatulovskiy, E., Tyson, R., Bretschneider, T., Kay, R.R., 2014. Bleb-driven chemotaxis of dictyostelium cells. J. Cell. Biol. 204 (6), 1027–1044.